*Conference Proceedings of the 5ᵗʰ Asia Pacific Luminescence and Electron Spin Resonance Dating Conference
October 15ᵗʰ-17ᵗʰ, 2018, Beijing, China*

Guest Editor: Liping Zhou

RESIDUAL DOSE OF K-FELDSPAR POST-IR IRSL OF BEACH-SHOREFACE SANDS AT KUJUKURI, EASTERN JAPAN

TORU TAMURA[1, 2], JUNKO KOMATSUBARA[1], SAIKO SUGISAKI[1] and NAOHISA NISHIDA[3]

[1]*Geological Survey of Japan, National Institute of Advanced Industrial Science and Technology, Tsukuba, Ibaraki, Japan*
[2]*Graduate School of Frontier Sciences, The University of Tokyo, 5 Chome-1-5 Kashiwanoha, Kashiwa, Chiba, Japan*
[3]*Department of Environmental Sciences, Tokyo Gakugei University, Koganei, Tokyo, Japan*

Abstract: We assessed the residual dose of K-feldspar grains from modern and Holocene beach–shoreface sands at Kujukuri, eastern Japan. Samples from the modern foreshore and shoreface (to 34 m depth) show residual doses <0.2 Gy for infrared-stimulated luminescence $(IR)_{50}$ measured during post-IR infrared-stimulated luminescence $(pIRIR)_{50/150}$, equivalent to potential burial age overestimation of only several decades for given dose rates. Residual doses of 1–3 Gy are retained by $pIRIR_{50/150}$, equivalent to 400–1,300 years; $pIRIR_{50/290}$ residual doses are up to 30 Gy, suggesting possible overestimation by >10,000 years. Residual doses of Holocene sands were also assessed by comparison with radiocarbon ages, revealing consistent results with modern sands. The $pIRIR_{50/290}$ results show no pronounced correlation of residual dose with water depth, except for a few samples from <5 m depth with residual doses several tens of per cent lower than those of deeper sands, suggesting that most samples were not fully bleached and that sustained subaerial sunlight bleaching diminishes the difficult-to-bleach component. Compared to the uncertainties associated with other factors, such as the fading correction, the residual doses of IR_{50} and $pIRIR_{50/150}$ are negligible for samples older than late and early Holocene, respectively. In contrast, the residual dose of $pIRIR_{50/290}$ may lead to critical age overestimation of Late Pleistocene deposits if the residual dose is not properly corrected.

Keywords: beach, feldspar, post-IR IRSL, residual dose, shallow marine.

1. INTRODUCTION

Feldspar infrared-stimulated luminescence (IRSL) and post-IR IRSL (pIRIR) are widely used for burial or depositional dating, in addition to quartz optically stimulated luminescence (OSL) (Thomsen *et al*., 2008; Buylaert *et al*., 2009, 2012). The dating protocols for feldspars are generally more complicated than those for quartz, but due to their higher level of signal saturation, they are applicable to older deposits than quartz OSL dating. Feldspars are also used as a dosimeter in cases where quartz OSL has properties unfavourable for dating (e.g., Preusser *et al*., 2014).

The prominent disadvantage of feldspar IRSL and pIRIR is, as well as anomalous fading (Li *et al*., 2014), the lower rate of sunlight bleaching compared to quartz, which likely results in residual dose and age overestima-

Corresponding author: T. Tamura
e-mail: toru.tamura@aist.go.jp

tions. The residual dose tends to be higher at higher measurement temperature and after higher preheat (Madsen *et al.*, 2011; Reimann and Tsukamoto, 2012; Fu and Li, 2013) and varies among samples (Li *et al.*, 2013) and sedimentary environments. Estimation of the residual dose is crucial for accurate feldspar dating and has been attempted by means of measurements of modern samples (e.g., Buylaert *et al.*, 2011; Brill *et al.*, 2018; Li *et al.*, 2018a), comparisons with other age estimates such as radiocarbon dating and quartz OSL (e.g., Li *et al.*, 2018b), and measurements of artificially bleached samples (e.g., Buylaert *et al.*, 2013). Case studies of such estimates are, however, limited compared with the variations of depositional environments that may greatly affect the residual dose, hindering the reliable application of feldspar IRSL and pIRIR dating.

Late Quaternary shallow-marine deposits are important components of continental margin geology. Glacial sea-level cycles have resulted in depositional sequences that provide archives of long-term environmental changes and tectonic histories (e.g., Murray-Wallace, 2002). Absolute dating of Middle to Late Pleistocene siliciclastic depositional systems is highly reliant on feldspar pIRIR dating because these deposits contain no material suitable for U/Th dating, and in many cases, are older than the applicable range of quartz OSL and radiocarbon dating. However, bleaching of luminescence signals in shallow-marine environments does not always occur because seawater strongly absorbs the ultraviolet component of sunlight (e.g., Rink and Pieper, 2001). Some previous studies of modern and Holocene sediments have empirically determined the degree of bleaching or the residual dose of quartz and feldspar luminescence in coastal shallow-marine settings (e.g., Roberts and Plater, 2007; Sugisaki *et al.*, 2015; Chamberlain *et al.*, 2017; Li *et al.*, 2018b; Nian *et al.*, 2018), but further efforts should be made to understand the variations related to a range of coastal systems.

We report the residual dose of IRSL and pIRIR at different temperatures observed for K-feldspar sand from the beach and shoreface on the Kujukuri coast, eastern Japan. Both modern and Holocene samples, which are compared with radiocarbon dating, were used to quantify the residual dose and examine the variation and trend within the coastal system. These results are useful for assessing the potential age overestimation from K-feldspar dating and for selecting the best signal to date Holocene and Pleistocene sediments, which especially promotes accurate dating of a thick forearc basin fill that accumulated since the Middle Pleistocene in the region.

2. STUDY AREA

The Kujukuri coast is part of the Pacific coast of the Boso Peninsula, eastern Japan (**Fig. 1A**). The area is a microtidal and open-ocean coast characterized by an arcuate 60-km-long sandy beach, shoreface, and shelf, bounded by headlands of Plio-Pleistocene sedimentary rocks to the northeast and southwest (Tamura *et al.*, 2008a). The tidal range is, on average, 107 cm, with a maximum value of 178 cm during the spring tide (Tamura *et al.*, 2008b). The mean significant wave height at the central Kujukuri coast is 1.0 m, with a wave period of 7.9 s (Nagai, 2002). During storm conditions, which occur several times per year, the hourly significant wave height exceeds 4 m and the typical wave period is 12 s (Tamura *et al.*, 2008a). The shoreface has multiple longshore bars at water depths of 0–6 m, and its average gradient is 1/150 at 0–5 m deep and 1/200 at 5–15 m deep.

An extensive beach-ridge plain is developed behind the Kujukuri coast. The landward margin of this plain is defined by plateaus and hills 30–120 m above sea level, and the surface of the plateaus corresponds to a raised marine terrace of the Last Interglacial Period (**Figs. 1B** and **2**; Unozawa *et al.*, 1983). The margin of the plain coincided with the shoreline at ca. 6 ka (Moriwaki, 1979; Masuda *et al.*, 2001a) when the post-glacial transgression culminated (**Fig. 2**). Since then, the shoreline has prograded, producing the present sequence of beach ridges that are 10 km wide at their widest point. Seven small rivers discharge into the sea through the beach-ridge plain but supply a limited amount of sediment to the coast. Instead, the rapid retreat of headlands at Byobugaura and Taitosaki (**Fig. 1B**) has created the sediment supply for the coastal progradation (Uda, 1989). Three beach-ridge assemblages are defined, which are referred to as groups I to III from land to sea. Detailed radiocarbon dating of the beach deposits clarified that beach-ridge groups I, II, and III formed at 5.7–4.0, 4.0–2.3, and after 2.3 ka, respectively (Masuda *et al.*, 2001b). At the northern end of the beach-ridge plain, a 10-km-wide relict lagoon forms a depression between the innermost beach ridge and the plateau (**Fig. 1B**).

The subsurface stratigraphy of the central part of the beach-ridge plain is constrained by a series of sediment cores and radiocarbon chronology; a 20-m-thick sandy body was deposited as part of the progradation of the beach–shoreface system, as can be observed in the present nearshore area, since 6 ka (Tamura *et al.*, 2003, 2007, 2008a, 2008b). The presence of a raised Pleistocene marine terrace nearby demonstrates that the Kujukuri coast has been uplifted. Masuda *et al.* (2001b) recognized a total sea-level fall of 5 m since 5.7 ka on the basis of the elevations of foreshore facies in the central coast; this sea-level fall was induced by a combination of tectonic uplift and hydro-isostasy (Nakada *et al.*, 1991). The longshore variation of the foreshore facies elevation indicates an increase in the uplift rate towards the southern end of the coast (Tamura *et al.*, 2010).
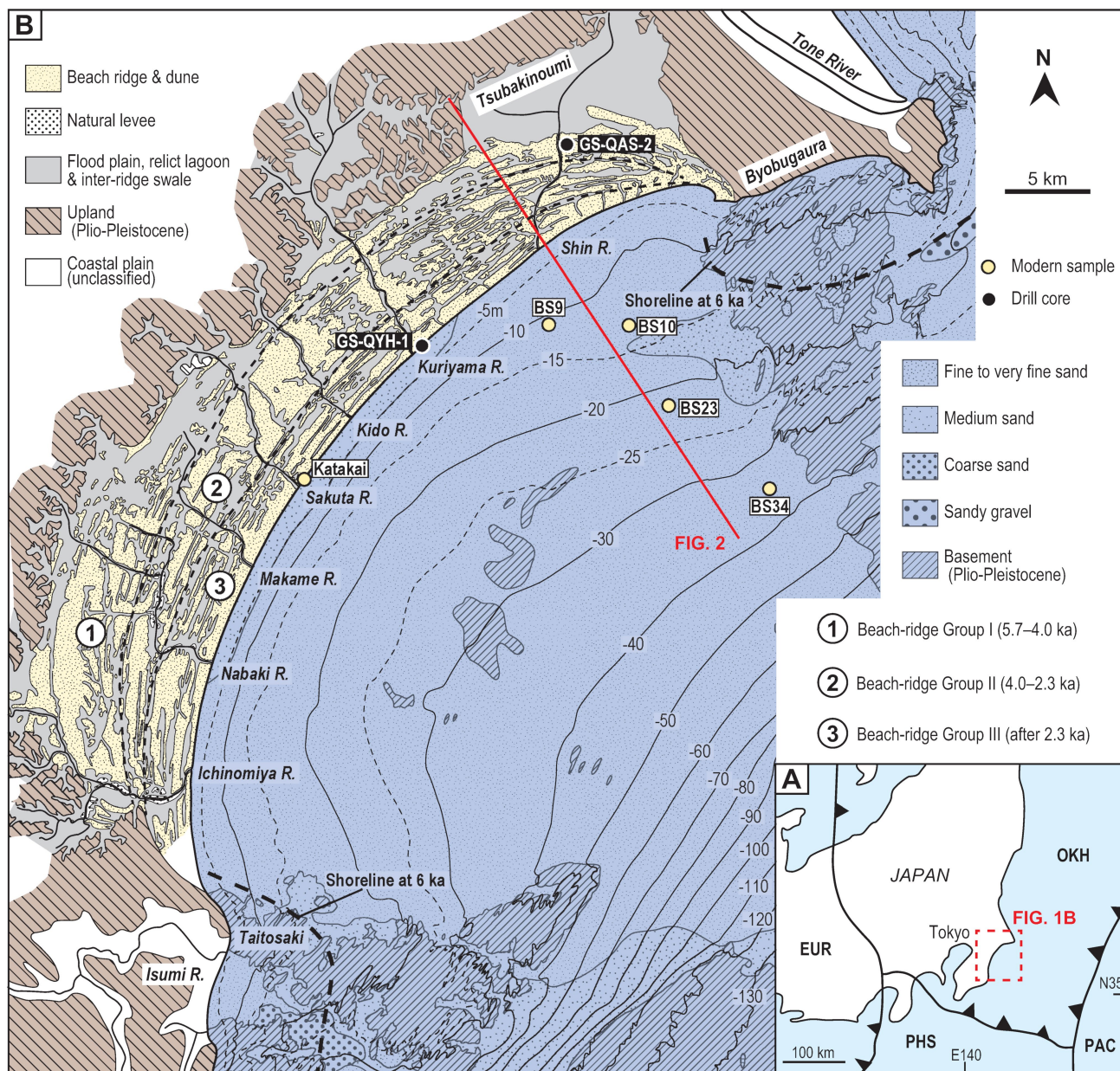
Fig. 1. *A) Location map of the study area and plate boundaries between the Eurasian (EUR), Okhotsk (OKH), Philippine Sea (PHS), and Pacific Ocean (PAC) plates. B) Morpho-sedimentary map of the Kujukuri beach-ridge plain and offshore showing the locations of modern samples and drill cores (modified from Tamura et al., 2008b). Five modern samples (Katakai, BS9, 10, 23, and 34) and two drill cores (GS-QYH-1 and GS-QAS-2) were used for the analysis. The red line shows the location of the cross section in Fig. 2. The definition of beach-ridge groups I–III is after Moriwaki (1979) and their formative durations were determined based on radiocarbon chronology in a cross section near the Makame and Sakuta rivers (Masuda et al., 2001b; Tamura et al., 2007).*
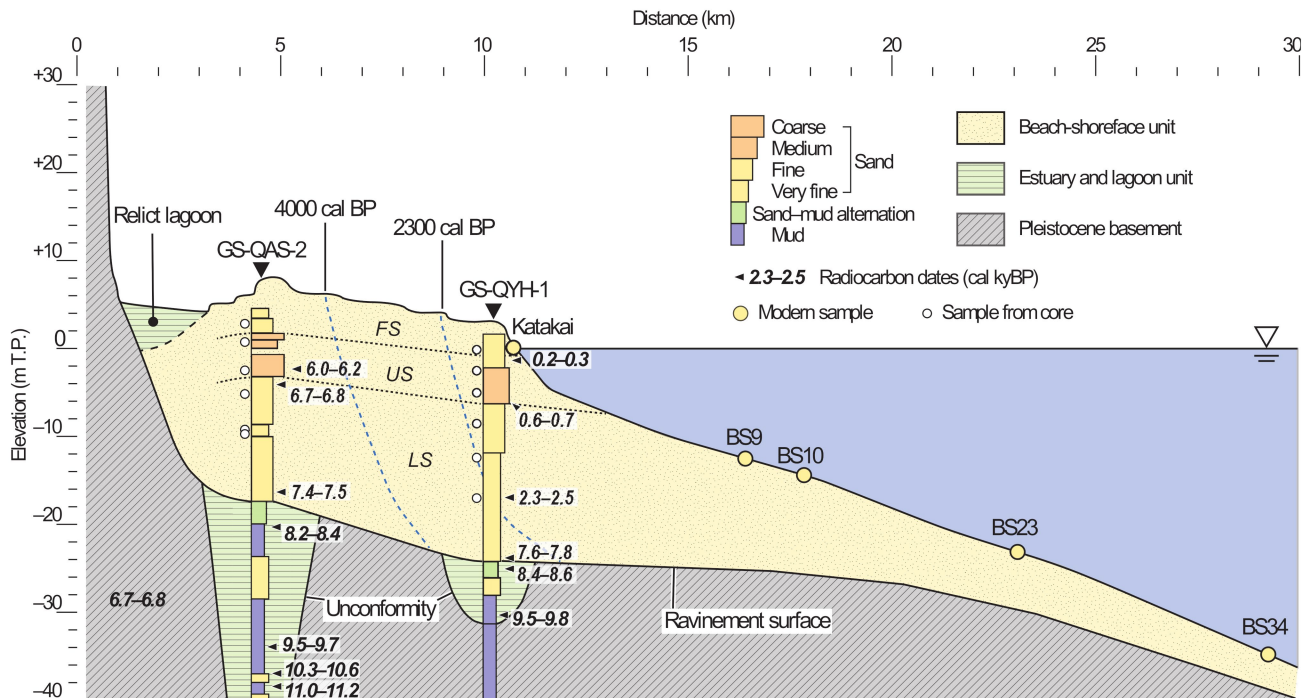
Fig. 2. *Cross section across the Kujukuri beach-ridge plain and offshore area (see location in Fig. 1b). The positions of the two drill cores and five modern sediment samples analyzed herein were projected onto a single section. Six samples were taken for analysis from each drill core. Radiocarbon dates of molluscan shells and a plant fragment are shown beside the columns of the cores. Dashed lines indicate the isochrones of the beach-ridge group boundary. The stratigraphic outline was defined on the basis of drill cores and compilations of previous studies in the central part of the plain (e.g., Tamura et al., 2003, 2007, 2008a, 2008b). FS: foreshore and backshore facies; US: upper shoreface facies; LS: lower shoreface facies; T.P.: Tokyo Peil, the standard datum for elevation measurements in Japan.*

3. SAMPLES AND METHODS

Modern samples

Sand samples for luminescence measurements were collected from the modern and Holocene beach and shoreface of the Kujukuri coast (**Fig. 1B**; **Tables 1** and **2**). A modern foreshore sample (gsj15160) was taken from the 5-cm-thick surface layer at Katakai, in the central part of the coast, using a light-tight plastic tube (**Table 1**). Four modern shoreface samples (gsj17282, 17283, 17284, and 17273) were scooped by the Smith–McIntyre sediment grab during a research cruise in August and September 2014 (Nishida *et al*., 2019). Plastic tubes >5 cm thick were hammered into the bulk sediment in the grab to collect light-unexposed sediments, which were transported to the laboratory.

Holocene samples

Two sediment cores (GS-QAS-2 and GS-QYH-1) were drilled in the northeastern part of the Kujukuri beach-ridge plain in 2015 (**Table 2**; Komatsubara, 2019). Cores GS-QAS-2 and GS-QYH-1 contained subsurface sediment successions representative of the landward and seaward parts of the prograded beach-ridge plains, respectively; both cores include the lower unit, consisting of the transgressive estuary and lagoon deposits in an incised valley, and the upper unit, containing regressive beach–shoreface deposits.

The upper unit of core GS-QAS-2 overlies and exhibits a gradual boundary with the incised-valley deposits at approximately 22.5 m depth and contains a succession of lower shoreface, upper shoreface, and foreshore and backshore facies, in ascending order. The lower shoreface facies occurs in the depth interval 8.2–22.5 m and consists of horizontally to low-angle cross-laminated very fine to fine sand. The upper shoreface facies is high-angle cross-laminated fine to very coarse sand in the depth range of 3.3–8.2 m. The foreshore and backshore facies is observed at 1.7–3.3 m depth and is characterized by horizontally laminated fine to medium sand with concentrations of heavy minerals. The upper unit of core GS-QYH-1, similarly to GS-QAS-2, consists of the lower shoreface (8.4–26.1 m depth), upper shoreface (3.0–8.4 m depth), and foreshore and backshore facies (0.5–3.0 m depth).

Six sand samples were taken from the upper units of each of the cores GS-QAS-2 and GS-QYH-1 (**Table 2**), yielding a total of 12 samples for OSL dating. Shell-rich layers were avoided in sampling to minimize the potential inaccuracy in dose-rate determination caused by the heterogeneous distribution of radionuclides in the sediment (e.g., Cunningham *et al*., 2019).

Table 1. *Details of modern samples. Equivalent doses (D_e) were determined from IR_{50}, $pIRIR_{150}$, and $pIRIR_{290}$.*

Site	Lab code	Latitude	Longitude	Water depth (m)	D_e from IR_{50} (Gy)	D_e from $pIRIR_{150}$ (Gy)	D_e from $pIRIR_{290}$ (Gy)
Katakai	gsj15160	N35°32'28.2"	E140°27'55.8"	0	0.09 ± 0.01	0.93 ± 0.08	11.93 ± 1.66
BS9	gsj17282	N35°37'42.1"	E140°37'13.9"	13	0.04 ± 0.01	1.80 ± 0.16	27.28 ± 1.08
BS10	gsj17283	N35°37'42.3"	E140°40'16.6"	14	0.07 ± 0.003	2.45 ± 0.13	29.09 ± 1.44
BS23	gsj17284	N35°35'11.9"	E140°41'48.5"	23	0.18 ± 0.01	3.25 ± 0.33	29.27 ± 1.47
BS34	gsj17273	N35°32'40.0"	E140°45'39.4"	34	0.06 ± 0.01	2.26 ± 0.14	23.92 ± 1.60

Table 2. *Details of Holocene samples taken from drill cores: sample level, water, U, Th, K, and Rb contents, estimated dose rates, and expected ages from radiocarbon dates. The internal dose rate was estimated to be 0.738±0.123 Gy/ka for all samples.*

Lab code	Depth (m)	Water content (%)	U (ppm)	Th (ppm)	K (%)	Rb (ppm)	Cosmic dose rate (Gy/ka)	Total dose rate (Gy/ka)	Expected age (ka)
GSJ-QAS2 (N35°43'17.3" E140°37'52.0" Elevation: +5.2 m)									
gsj15149	2.2	21	0.67	2.9	1.1	39	0.15 ± 0.02	2.07 ± 0.14	5.89 ± 0.08
gsj15151	4.2	31	0.89	3.6	1.3	48	0.12 ± 0.01	2.17 ± 0.14	6.01 ± 0.08
gsj15154	7.5	20	0.7	3.0	1.4	55	0.09 ± 0.01	2.28 ± 0.14	6.26 ± 0.08
gsj15155	10.2	39	1.1	4.3	1.6	62	0.07 ± 0.01	2.26 ± 0.14	6.88 ± 0.08
gsj15157	14.4	34	0.89	3.8	1.6	60	0.05 ± 0.01	2.28 ± 0.14	7.13 ± 0.08
gsj15158	14.8	42	1.2	3.8	1.6	62	0.05 ± 0.00	2.21 ± 0.14	7.15 ± 0.08
GSJ-QYH1 (N35°37'00.0" E140°32'29.2" Elevation: +2.1 m)									
gsj15254	2.3	20	0.91	4.8	0.97	34	0.15 ± 0.02	2.13 ± 0.14	0.23 ± 0.08
gsj15255	4.9	33	0.88	3.1	1.6	58	0.11 ± 0.01	2.30 ± 0.14	0.45 ± 0.08
gsj15256	7.2	30	0.67	3.3	1.5	52	0.09 ± 0.01	2.23 ± 0.14	0.66 ± 0.08
gsj15257	10.7	33	0.76	4.0	1.5	50	0.06 ± 0.01	2.16 ± 0.14	1.13 ± 0.08
gsj15258	14.6	31	0.73	3.1	1.6	50	0.05 ± 0.01	2.21 ± 0.14	1.74 ± 0.08
gsj15259	19.2	31	0.8	3.5	1.6	51	0.03 ± 0.00	2.24 ± 0.14	2.44 ± 0.08

Radiocarbon dating

Accelerator mass spectrometry radiocarbon dating of shells and plant fragments from the sediment cores was performed by the Institute of Accelerator Analysis Ltd. (Kawasaki City, Japan) to establish an independent chronology for comparison with the OSL dating results (**Table 3**). Six intact shells and one plant fragment sample were dated for core GS-QAS-2, and six intact shells were analyzed for core GS-QYH-1. The ages obtained were converted into calendar ages by the program CALIB rev. 7.1.0 (Stuiver and Reimer, 1993) using the data set MARINE13 with a delta R of 0 years for the shell samples and INTCAL13 for the plant fragment sample (Reimer *et al.*, 2013).

The radiocarbon ages are consistent with the stratigraphy in both cores (**Figs. 2** and **3**). In the lower unit of core GS-QAS-2, four samples were dated between 10,878–10,933 cal BP and 8,224–8,388 cal BP, supporting the interpretation of transgressive deposition. Likewise, two radiocarbon ages from the lower unit of GS-QYH-1 indicate the occurrence of transgressive deposition. Three ages from the upper unit of GS-QAS-2 range from 7,411–7,540 to 6,019–6,239 cal BP, corresponding to the initial regressive phase. The upper unit of GS-QYH-1 was dated as Late Holocene. Cores GS-QAS-2 and GS-QYH-1 thus represent the middle and late Holo-cene regressive succession of a prograding beach–shoreface deposit (**Fig. 2**).

Radiocarbon ages were used to define the expected ages of the Holocene samples taken from the cores (**Table 2**). The expected age of an OSL sample was obtained by linear interpolation of the intercepts of 2σ radiocarbon ages just above and below the sample and was associated with the mean uncertainties of the 2σ radiocarbon ages. For interpolation above the uppermost radiocarbon age, the dates of the tops of cores GS-QAS-2 and QYH-1 were assumed to be 5.7 ka and 0 ka, respectively.

Luminescence dating

Sample preparation and luminescence measurements were performed at the luminescence laboratory of the Geological Survey of Japan. Samples taken from drill cores were split into two, with one part used for luminescence measurements and the other for dosimetry; the modern samples were exclusively used for luminescence measurements. Samples for luminescence measurements were processed under subdued red light to avoid depletion of the luminescence signal. They were dried, sieved to extract grains 180–250 µm in diameter, and then treated with hydrochloric acid and hydrogen peroxide to remove carbonate and organic matter. Quartz and feldspar grains were then separated using sodium polytungstate
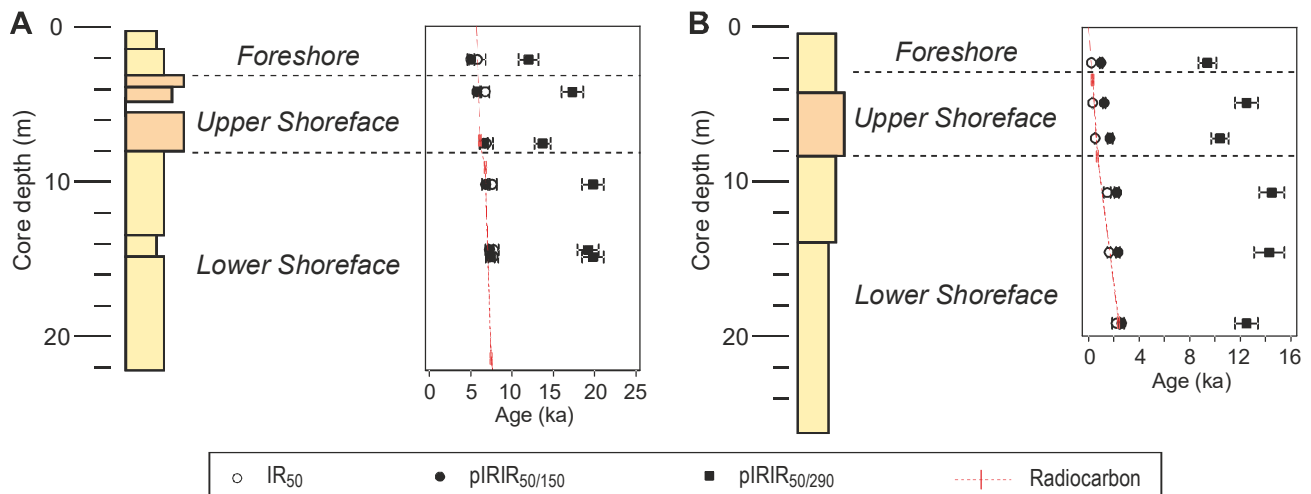
Fig. 3. *Fading-corrected final luminescence age estimates of samples taken from (A) core GS-QAS-2 and (B) core GS-QYH-1. Radiocarbon ages of molluscan shells are also shown for comparison. Radiocarbon ages at the ground surface were assumed to be 5.7 ka and 0 ka for cores GS-QAS-2 and GS-QYH-1, respectively, to define the expected ages (red lines).*

Table 3. *Radiocarbon dating results for drill core samples.*

Access code	Core depth (m)	Sample	Conventional ^{14}C age (yr BP)	Calibrated age (2s) (cal yr BP)	Probability
GS-QAS-2					
IAAA-153551	7.3	Shell (*Mactra chinensis*)	5720 ± 30	6019–6239	1.000
IAAA-153282	9.1	Shell (*M. chinensis*)	6290 ± 30	6653–6843	1.000
IAAA-153552	21.3	Shell (*Raetellops pulchellus*)	6970 ± 30	7411–7540	1.000
IAAA-153283	25.4	Shell (*R. pulchellus*)	7850 ± 30	8224–8388	1.000
IAAA-153284	38.9	Shell (*Glossaulax didyma*)	8950 ± 30	9511–9708	1.000
IAAA-153553	41.8	Shell (*Dosinia angulosa*)	9570 ± 40	10295–10551	1.000
IAAA-151461	43.6	Plant fragment	9700 ± 40	10878–10933	0.097
				11080–11212	0.903
GS-QYH-1					
IAAA-153560	3.4	Shell (*Chion semigranosa*)	620 ± 20	146–164	0.026
				187–312	0.974
IAAA-153288	8.4	Shell (*M. chinensis*)	1150 ± 20	649–749	1.000
IAAA-153561	19.1	Shell (*Siliqua pulchella*)	2680 ± 30	2303–2456	1.000
IAAA-153289	25.8	Shell (*R. pulchellus*)	7220 ± 30	7596–7761	1.000
IAAA-153562	27.3	Shell (*Macoma tokyoensis*)	8020 ± 30	8393–8556	1.000
IAAA-153290	32.4	Shell (*Dentalium octangulatum*)	9010 ± 40	9540–9822	1.000

liquids of densities 2.70, 2.58, and 2.53 g/cm^3. The 2.53–2.58 g/cm^3 fraction was taken as K-feldspar. Quartz samples were purified by etching the 2.58–2.70 g/cm^3 fraction in 40% hydrofluoric acid for 1 h, followed by hydrochloric acid treatment for 1 h. Grains were mounted on stainless steel disks to form large (6 mm diameter) aliquots for luminescence measurement. Measurements were performed with a TL-DA-20 automated Risø TL/OSL reader equipped with blue and infrared LEDs centred on wavelengths of 470 and 970 nm, respectively, for stimulation and a ^{90}Sr/^{90}Y beta source for laboratory irradiation. For stimulation by blue and infrared LEDs, emitted luminescence through a Hoya U-340 filter and a combination of Schott BG3 (3 mm thick), BG39 (2 mm),

and GG400 (3 mm) filters was measured with a photomultiplier tube. Preliminary measurements showed that natural quartz OSL signals are dominated by the medium component and not appropriate for dating, as is also the case for other quartz sands in Japan (e.g., Tsukamoto *et al.*, 2003; Tokuyasu *et al.*, 2010; Tamura *et al.*, 2015, 2017; Riedsel *et al.*, 2018); therefore, only the IRSL and pIRIR signals of the K-feldspar grains were further investigated.

The modified single-aliquot regenerative dose protocols of pIRIR measured at 150°C and 290°C after a prior IRSL at 50°C (referred to here as pIRIR$_{150}$ and pIRIR$_{290}$, respectively; **Table 4**; Thomsen *et al.*, 2008; Buylaert *et al.*, 2009, 2012; Reimann and Tsukamoto, 2012) were

Table 4. *Summaries of the IR$_{50}$, pIRIR$_{150}$, and pIRIR$_{290}$ single-aliquot regenerative dose protocols used in this study.*

Step	post-IR IRSL (150°C)	Signal	post-IR IRSL (290°C)	Signal
1	Preheat at 180°C for 60 s		Preheat at 320°C for 60 s	
2	IR stimulation at 50°C for 100 s	Lx for IRSL50	IR stimulation at 50°C for 200 s	
3	IR stimulation at 150°C for 100 s	Lx for post-IR IRSL150	IR stimulation at 290°C for 200 s	Lx for post-IR IRSL290
4	Test dose		Test dose	
5	Preheat at 180°C for 60 s		Preheat at 320°C for 60 s	
6	IR stimulation at 50°C for 100 s	Tx for IRSL50	IR stimulation at 50°C for 200 s	
7	IR stimulation at 150°C for 100 s	Tx for post-IR IRSL150	IR stimulation at 290°C for 200 s	Tx for post-IR IRSL290
8	Dose and return to step 1		IR stimulation at 325°C for 200 s	
9			Dose and return to step 1	

applied to the K-feldspar grains. The prior IRSL signal in the pIRIR$_{150}$ protocol was also investigated and is referred to here as IR$_{50}$. In the pIRIR$_{150}$ protocol, the IR$_{50}$ and pIRIR$_{150}$ signals were sampled every 0.1 s for 100 s, and the net signal was derived from the integral of the first 2.0 s of the signal after subtracting the background estimated from the last 20 s of the signal. The pIRIR$_{290}$ signal was sampled every 0.1 s for 200 s with signal and subtraction integration intervals of the first 2.0 s and last 20 s, respectively. Preheat temperatures were fixed at 180°C for 60 s for pIRIR$_{150}$ and 320°C for 60 s for pIRIR$_{290}$. Bleaching experiments and dose recovery tests were practised for sample gsj15151. Six aliquots for each protocol were exposed to artificial sunlight for 4 h in a UVACUBE 400 chamber (Hönle) with an SOL 500 lamp module. After bleaching, three aliquots were dosed by 24 Gy for pIRIR$_{150}$ and by 72 Gy for pIRIR$_{290}$, and then used for a dose recovery test; the remaining aliquots were used to estimate the residual dose. Dose recovery was assessed after subtracting the residual dose from the recovered dose. IR$_{50}$, pIRIR$_{150}$, and pIRIR$_{290}$ yielded recovery ratios of 0.97±0.01, 0.96±0.02, and 1.17±0.08, respectively. The residual doses observed in the bleaching test were 0.31±0.09, 1.51±0.17, and 13.66±1.10 Gy for IR$_{50}$, pIRIR$_{150}$, and pIRIR$_{290}$, respectively. The mean value of the equivalent dose was determined from measurements of six replicates per sample by applying the Central Age Model of Galbraith *et al.* (1999). For all samples except gsj15151, 15155, 15157, and 15158, fading tests were also performed on aliquots after equivalent dose measurement to determine fading rates (expressed as the g$_{2days}$-value) following the method of Auclair *et al.* (2003).

For drill core samples, the environmental dose rate was determined using the DRAC program of Durcan *et al.* (2015) based on the contributions of both natural radioisotopes and cosmic radiation (**Table 2**). The concentrations of K and U were measured by inductively coupled plasma optical emission spectrometry and those of Th and Rb by inductively coupled plasma mass spectrometry; both sets of results were converted to dose rates by applying to the conversion factors of Adamiec and Aitken

(1998). The attenuation factors used for beta and alpha rays were based on Mejdahl (1979) and Bell (1980), respectively. We used an a-value of 0.15±0.05 (Balescu and Lamothe, 1994). The a-values for IRSL and pIRIR signals are generally considered variable (e.g., Kreutzer *et al.*, 2014); however, potential uncertainties in total dose rate related to the a-value are not significant (less than a few per cent), and thus we assume an identical a-value for IRSL and pIRIR. The internal K content of K-feldspar was assumed to be 12.5±0.5% (Huntley and Baril, 1997). The water content was also considered for the dose rate determination based on the measured value with an error of 5%. The cosmic dose rate was estimated based on Prescott and Hutton (1994) assuming overburden with a density of 1.8 g/cm^3. The mean equivalent dose values were divided by the environmental dose rate to obtain fading-uncorrected ages. Mean g-values determined from six aliquots per sample and their standard errors for each signal were used for fading corrections of uncorrected ages based on Huntley and Lamothe (2001) and using the R Luminescence Package (Kreutzer *et al.*, 2012; Fuchs *et al.*, 2015). For correction of the four samples on which no fading test was performed, the average of the rest of the samples was applied. All dates are expressed relative to AD 2015.

4. RESULTS

Modern samples

In all modern samples, a bright natural pIRIR$_{290}$ signal was observed, whereas the IR$_{50}$ and pIRIR$_{150}$ signals were generally weak compared to the pIRIR$_{290}$ signal (**Fig. 4A**). Nevertheless, a dose–response curve was well defined for each signal, from which the equivalent dose was estimated. Equivalent doses of IR$_{50}$ were <0.1 Gy except for sample gsj17284, taken at a water depth of 23 m, which retains a residual dose of 0.18±0.01 Gy. The pIRIR$_{150}$ signal yielded higher residual doses than the IR$_{50}$, ranging from 0.93 to 3.25 Gy. The residual doses of pIRIR$_{290}$ were much higher than pIRIR$_{150}$: they were 11.93±1.66 Gy for the foreshore sample (gsj15160) at Katakai and 23–30 Gy for other subtidal samples.
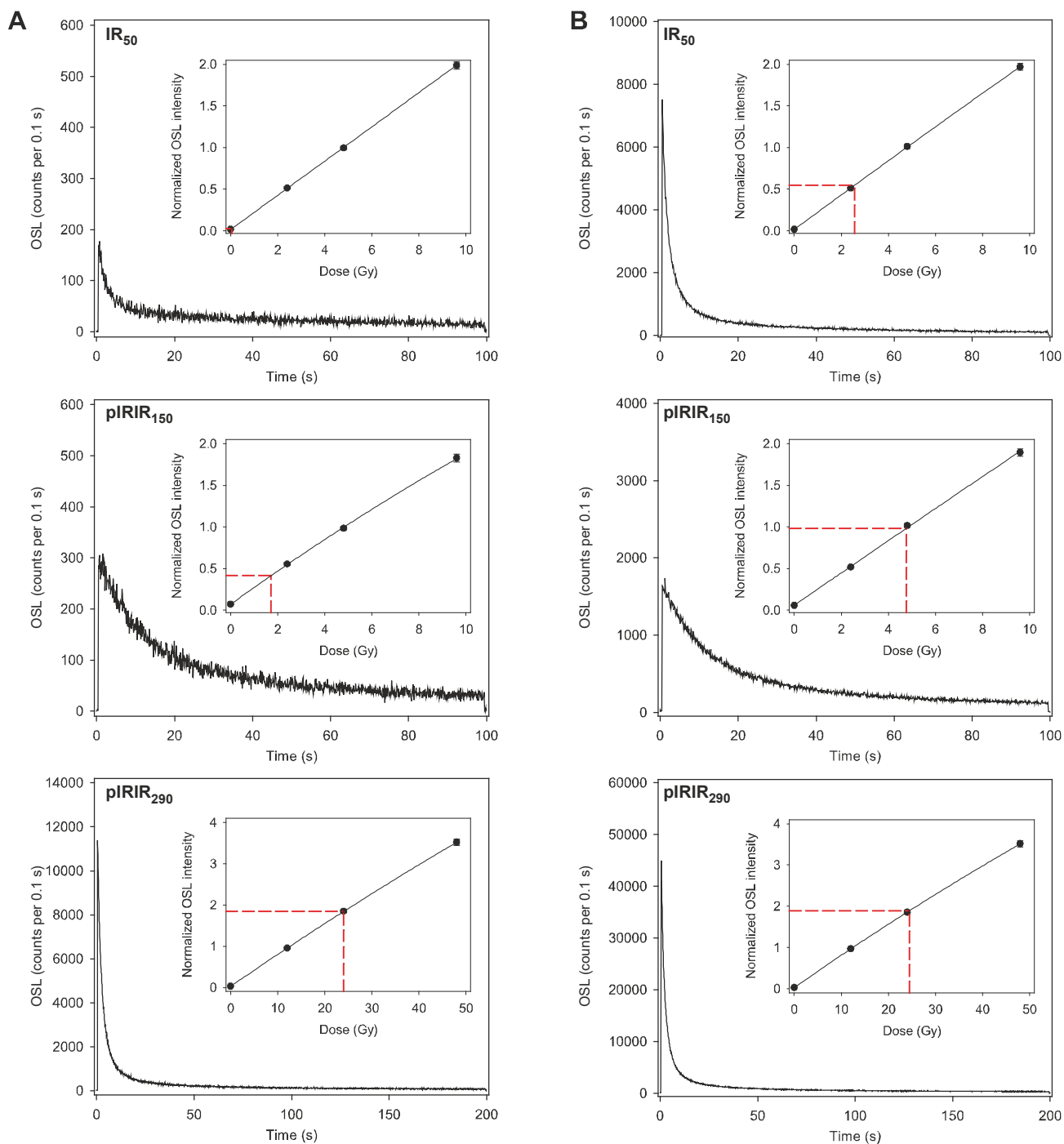
Fig. 4. *Decay curves and dose–response curves (inset) of IR$_{50}$, pIRIR$_{150}$, and pIRIR$_{290}$ measured on samples (A) gsj15259 and (B) gsj17282. The intersections of the natural OSL intensity with the dose–response curve and the corresponding equivalent dose are highlighted with red dashed lines.*

Equivalent dose and burial age estimate of Holocene samples

Bright natural IR_{50} and $pIRIR_{150}$ signals, as well as bright $pIRIR_{290}$ signal, were observed for Holocene samples (**Fig. 4B**). Equivalent doses were estimated from well-defined dose–response curves. Equivalent doses of IR_{50} decrease upwards in both cores, ranging from 5.25 to 8.10 Gy in core GS-QAS-2 and from 0.28 to 2.49 Gy in GS-QYH-1 (**Table 5**). Equivalent doses of $pIRIR_{150}$ also decrease upwards, and are higher than the equivalent doses of IR_{50} in all samples. In contrast, the $pIRIR_{290}$ signal yields much higher equivalent doses than $pIRIR_{150}$, and does not show systematic trends in either core. Average g-values of IR_{50} were high (7.96 ± 0.15%/decade), whereas those of $pIRIR_{150}$ and $pIRIR_{290}$ were as low as 1.21 ± 0.11%/decade and 1.28 ± 0.09%/decade, respectively (**Fig. 5**).

In both cores, fading-corrected burial age estimates from IR_{50} and $pIRIR_{150}$ display consistent trends with the stratigraphy, whereas those from $pIRIR_{290}$ exhibit remarkable reversals (**Tables 5–7**, **Fig. 3**). Estimated dose rates were consistent, characterized by a small range of 2.07–2.30 Gy/ka. Fading-corrected ages of IR_{50} show vertical sequences from 7.7 to 5.8 ka in core GS-QAS and from 2.2 to 0.24 ka in core QYH-1, consistent with the stratigraphy (**Fig. 3**). The $pIRIR_{150}$ results also exhibited stratigraphically consistent trends of fading-corrected ages, but their ages are generally older than those of IR_{50} by up to 1,200 years in core GS-QYH-1. In core GS-QAS-2, the $pIRIR_{150}$ ages are, although overlapping with-

Table 5. *Equivalent dose (D_e), uncorrected age, g-value, corrected age, offset from expected age, and D_e offset from expected for IR_{50} signals of Holocene samples.*

Lab code	Depth (m)	D_e (Gy)	Uncorrected age (ka)	g-value (%/decade)	Corrected age (ka)	Age offset from expected (ka)	D_e offset from expected (Gy)
GS-QAS-2							
gsj15149	2.2	5.25 ± 0.09	2.5 ± 0.2	8.48 ± 0.73	5.8 ± 1.0	−0.1 ± 1.0	−0.17 ± 0.14
gsj15151	4.2	6.78 ± 0.11	3.1 ± 0.2	7.96 ± 0.15*	6.8 ± 0.5	0.8 ± 0.5	1.6 ± 0.07
gsj15154	7.5	7.64 ± 0.20	3.4 ± 0.2	7.51 ± 0.45	6.9 ± 0.8	0.6 ± 0.8	1.5 ± 0.11
gsj15155	10.2	7.89 ± 0.13	3.5 ± 0.2	7.96 ± 0.15*	7.6 ± 0.5	0.7 ± 0.5	1.6 ± 0.07
gsj15157	14.4	8.10 ± 0.09	3.6 ± 0.2	7.96 ± 0.15*	7.8 ± 0.6	0.6 ± 0.6	1.5 ± 0.09
gsj15158	14.8	7.82 ± 0.11	3.5 ± 0.2	7.96 ± 0.15*	7.7 ± 0.6	0.6 ± 0.6	1.3 ± 0.08
GS-QYH-1							
gsj15254	2.3	0.28 ± 0.01	0.13 ± 0.01	8.21 ± 0.42	0.2 ± 0.0	0.0 ± 0.1	0.01 ± 0.01
gsj15255	4.9	0.40 ± 0.01	0.18 ± 0.01	8.26 ± 0.28	0.3 ± 0.0	−0.1 ± 0.1	−0.29 ± 0.01
gsj15256	7.2	0.67 ± 0.02	0.30 ± 0.02	7.39 ± 0.10	0.5 ± 0.0	−0.1 ± 0.1	−0.27 ± 0.01
gsj15257	10.7	1.46 ± 0.03	0.68 ± 0.05	8.93 ± 0.90	1.5 ± 0.3	0.4 ± 0.3	0.77 ± 0.04
gsj15258	14.6	1.95 ± 0.02	0.88 ± 0.06	7.20 ± 0.13	1.6 ± 0.1	−0.1 ± 0.1	−0.26 ± 0.02
gsj15259	19.2	2.49 ± 0.03	1.1 ± 0.1	7.73 ± 0.73	2.2 ± 0.3	−0.3 ± 0.3	−0.57 ± 0.05

Table 6. *Equivalent dose (D_e), uncorrected age, g-value, corrected age, offset from expected age, and D_e offset from expected for $pIRIR_{150}$ signals of Holocene samples.*

Lab code	Depth (m)	D_e (Gy)	Uncorrected age (ka)	g-value (%/decade)	Corrected age (ka)	Age offset from expected (ka)	D_e offset from expected (Gy)
GS-QAS-2							
gsj15149	2.2	9.63 ± 0.35	4.7 ± 0.4	1.05 ± 0.38	5.0 ± 0.4	−0.9 ± 0.4	−1.82 ± 0.06
gsj15151	4.2	11.43 ± 0.46	5.3 ± 0.4	1.21 ± 0.11*	5.7 ± 0.4	−0.3 ± 0.4	−0.6 ± 0.05
gsj15154	7.5	13.53 ± 0.25	5.9 ± 0.4	1.32 ± 0.15	6.6 ± 0.5	0.3 ± 0.5	0.7 ± 0.07
gsj15155	10.2	14.12 ± 0.34	6.2 ± 0.4	1.21 ± 0.11*	6.8 ± 0.5	−0.1 ± 0.5	−0.1 ± 0.07
gsj15157	14.4	15.15 ± 0.45	6.7 ± 0.5	1.21 ± 0.11*	7.3 ± 0.5	0.1 ± 0.5	0.3 ± 0.07
gsj15158	14.8	14.89 ± 0.42	6.7 ± 0.5	1.21 ± 0.11*	7.4 ± 0.5	0.2 ± 0.5	0.5 ± 0.07
GS-QYH-1							
gsj15254	2.3	1.93 ± 0.12	0.9 ± 0.1	1.37 ± 0.70	1.0 ± 0.1	0.8 ± 0.1	1.60 ± 0.02
gsj15255	4.9	2.62 ± 0.12	1.1 ± 0.1	1.30 ± 0.14	1.2 ± 0.1	0.8 ± 0.1	1.83 ± 0.02
gsj15256	7.2	3.62 ± 0.35	1.6 ± 0.2	0.78 ± 0.18	1.7 ± 0.2	1.0 ± 0.2	2.34 ± 0.03
gsj15257	10.7	4.47 ± 0.29	2.1 ± 0.2	1.15 ± 0.14	2.2 ± 0.2	1.1 ± 0.2	2.40 ± 0.03
gsj15258	14.6	4.73 ± 0.11	2.1 ± 0.1	1.25 ± 0.15	2.3 ± 0.2	0.6 ± 0.2	1.32 ± 0.02
gsj15259	19.2	5.31 ± 0.15	2.4 ± 0.2	1.48 ± 0.27	2.6 ± 0.2	0.2 ± 0.2	0.42 ± 0.03

Table 7. *Equivalent dose (D_e), uncorrected age, g-value, corrected age, offset from expected age, and D_e offset from expected for pIRIR$_{150}$ signals of Holocene samples.*

Lab code	Depth (m)	D_e (Gy)	Uncorrected age (ka)	g-value (%/decade)	Corrected age (ka)	Age offset from expected (ka)	D_e offset from expected (Gy)
GS-QAS-2							
gsj15149	2.2	22.83 ± 1.25	11.0 ± 0.9	1.13 ± 0.17	12.0 ± 1.2	6.1 ± 1.2	12.64 ± 0.16
gsj15151	4.2	34.00 ± 1.51	15.7 ± 1.2	1.28 ± 0.09*	17.3 ± 1.3	11.3 ± 1.3	24.46 ± 0.18
gsj15154	7.5	28.50 ± 1.17	12.5 ± 0.9	1.16 ± 0.08	13.7 ± 1.0	7.4 ± 1.0	16.88 ± 0.15
gsj15155	10.2	40.57 ± 1.17	17.9 ± 1.2	1.28 ± 0.09*	19.8 ± 1.3	12.9 ± 1.3	29.21 ± 0.18
gsj15157	14.4	39.51 ± 1.36	17.3 ± 1.2	1.28 ± 0.09*	19.2 ± 1.3	12.0 ± 1.3	27.40 ± 0.19
gsj15158	14.8	39.62 ± 1.03	17.9 ± 1.2	1.28 ± 0.09*	19.8 ± 1.3	12.7 ± 1.3	27.95 ± 0.18
GS-QYH-1							
gsj15254	2.3	18.08 ± 0.60	8.5 ± 0.6	1.45 ± 0.37	9.4 ± 0.7	9.2 ± 0.7	19.58 ± 0.10
gsj15255	4.9	26.42 ± 1.38	11.5 ± 0.9	1.11 ± 0.16	12.5 ± 0.9	12.0 ± 0.9	27.69 ± 0.12
gsj15256	7.2	21.50 ± 0.85	9.6 ± 0.7	1.05 ± 0.32	10.4 ± 0.7	9.8 ± 0.7	21.78 ± 0.10
gsj15257	10.7	28.89 ± 0.79	13.4 ± 0.9	1.07 ± 0.12	14.5 ± 1.0	13.3 ± 1.0	28.85 ± 0.14
gsj15258	14.6	26.99 ± 1.02	12.2 ± 0.9	1.96 ± 0.36	14.3 ± 1.2	12.6 ± 1.2	27.81 ± 0.17
gsj15259	19.2	25.46 ± 0.64	11.4 ± 0.8	1.31 ± 0.18	12.5 ± 0.9	10.1 ± 0.9	22.66 ± 0.13
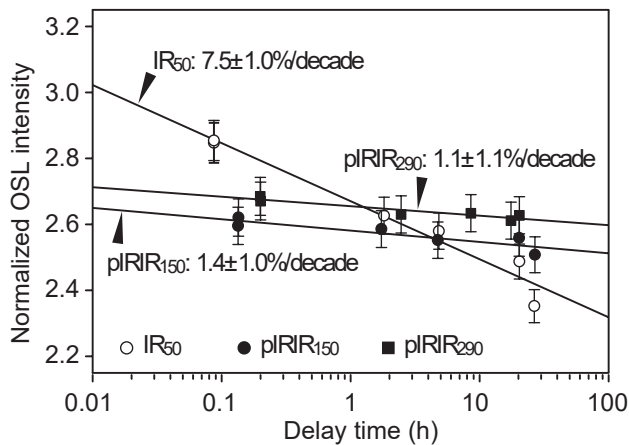
Fig. 5. *Fading test results of IR$_{50}$, pIRIR$_{150}$, and pIRIR$_{290}$ signals measured for sample gsj15258. A regression line was defined for each signal based on the least-squares method and then applied to estimate the g-value.*

in error, generally younger than the IR$_{50}$ ages. As expected from the equivalent dose, the fading-corrected ages of pIRIR$_{290}$ were inconsistent with the stratigraphy and older than 9 ka. However, it is noteworthy that the corrected pIRIR$_{290}$ ages in core GS-QAS-2 are generally older than those in core GS-QYH1 by several thousand years.

5. DISCUSSION

Residual dose characterization

As the five modern samples are supposed to have burial ages of 0 years, their equivalent doses are equal to the residual dose. The residual doses of IR$_{50}$ observed in the modern samples are less than 0.2 Gy, equivalent to only several decades for the given dose rate (**Table 2**). In contrast, pIRIR$_{50/150}$ retains residual doses of 1–3 Gy, equivalent to 400–1,300 years.

Characterization of residual doses for Holocene samples requires comparison with the expected ages obtained from radiocarbon dating. In core GS-QYH-2, fading-corrected IR$_{50}$ ages are consistent with radiocarbon ages. The radiocarbon ages of marine shells are likely older than the depositional ages as shells are not always buried immediately after their death; however, previous attempts confirmed that selective dating of intact shells results in consistent and precise chronology (Tamura *et al.*, 2003, 2007) and thus minimizes the potential age overestimation. In core GS-QAS-2, which comprises early to middle Holocene deposits, the IR$_{50}$ ages appear to be generally older than the expected ages derived from radiocarbon dating. The g-values determined here are higher than those of the majority of K-feldspar samples from other regions (Li *et al.*, 2014), which may have resulted in a slight inaccuracy of the ages in core GS-QAS-2. The opposite trend is identified for pIRIR$_{150}$ ages: the ages are older than the expected ages in core GS-QYH-1 and consistent with the expected ages in core GS-QAS-2. This finding suggests two possibilities: that either slight under-correction of the pIRIR$_{150}$ ages was caused by an underestimation of the g-value, which cancels residual doses, or the residual doses were negligible compared with the accuracy of ages determined for the early to middle Holocene deposits. Despite these slight discrepancies, these results show that the fading-corrected IR$_{50}$ and pIRIR$_{150}$ ages in the present study provide a consistent chronology that is at least as accurate as radiocarbon dating. This finding is regionally important because it demonstrates that for dating young sediments, the IR$_{50}$ and pIRIR$_{150}$ of K-feldspar can be an effective alternative for quartz OSL, which many studies have shown to be

inappropriate for dating in the Japanese archipelago (e.g., Tsukamoto *et al.*, 2003; Tokuyasu *et al.*, 2010; Tamura *et al.*, 2015, 2017; Riedsel *et al.*, 2018).

Appreciable residual doses were observed for the pIRIR$_{290}$ signal of modern samples up to 30 Gy (**Table 1**). Holocene samples also show much older age estimates of pIRIR$_{290}$ than expected, which is attributed to the residual dose. The residual dose of Holocene samples, D$_{residual}$, is defined as:

$$D_{residual} = (T_{osl} - T_{expected}) \times \dot{D} \qquad (5.1)$$

where T$_{osl}$ is the fading-corrected age estimate from pIRIR or IR$_{50}$, T$_{expected}$ is the expected age, and $\dot{D}$ is the dose rate. Residual doses are provided in **Tables 5–7** for each signal. The Holocene samples yielded residual doses of pIRIR$_{290}$ that were similar to those of modern samples, ranging from 20 to 29 Gy (**Table 7**).

Plots of fading-corrected equivalent doses D$_e$ (= T$_{osl} \times \dot{D}$) against expected D$_e$ (= T$_{expected} \times \dot{D}$) visualize the residual dose as a departure from the 1:1 line (**Fig. 6**). Although pIRIR$_{290}$ shows a larger scatter, its trend is distinct from that of the 1:1 line, and the y-intercept of the regression line of these plots indicates the average residual dose (e.g., Sohbati *et al.*, 2011), which is 24.2 Gy (**Fig. 6C**). In contrast, as expected from the age results, the corrected D$_e$ values of pIRIR$_{150}$ are consistent with the expected values, and only modern and late Holocene samples show identifiable departures from the 1:1 line (**Fig. 6B**). The departure of the IR$_{50}$ D$_e$ from the 1:1 line is only identified for early Holocene samples and possibly results from over-correction (**Fig. 6A**).

The average residual doses of pIRIR$_{290}$ are equivalent to an overestimate of 11,000 years, assuming an average dose rate of 2.2 Gy/ka. This overestimate leads to significant inaccuracy in dating Holocene sediments and possibly causes considerable overestimation even for deposits formed during the Last Interglacial Periods if the residual dose is not taken into account appropriately. No appreciable difference in the average g-value was identified between pIRIR$_{150}$ and pIRIR$_{290}$. If these g-values also apply for Late Pleistocene sediments, the lower residual dose of pIRIR$_{150}$ is an obvious advantage. However, an underestimated g-value of pIRIR$_{150}$ is also inferred from the apparent consistency of the pIRIR$_{150}$ ages with the expected ages for lower Holocene deposits in core GS-QAS-2, despite the influence of the residual dose. This possible inaccuracy in fading correction likely leads to large errors in dating older sediments. In selecting an optimal signal for feldspar dating, the g-value should also be carefully examined.

Correlation of residual dose with water depth

Saltwater absorbs the ultraviolet component of sunlight; thus, in shallow-marine environments, the bleachability of the luminescence signal is expected to rapidly drop as the water depth increases. However, the residual doses of IR$_{50}$ and pIRIR$_{150}$ in five modern samples show
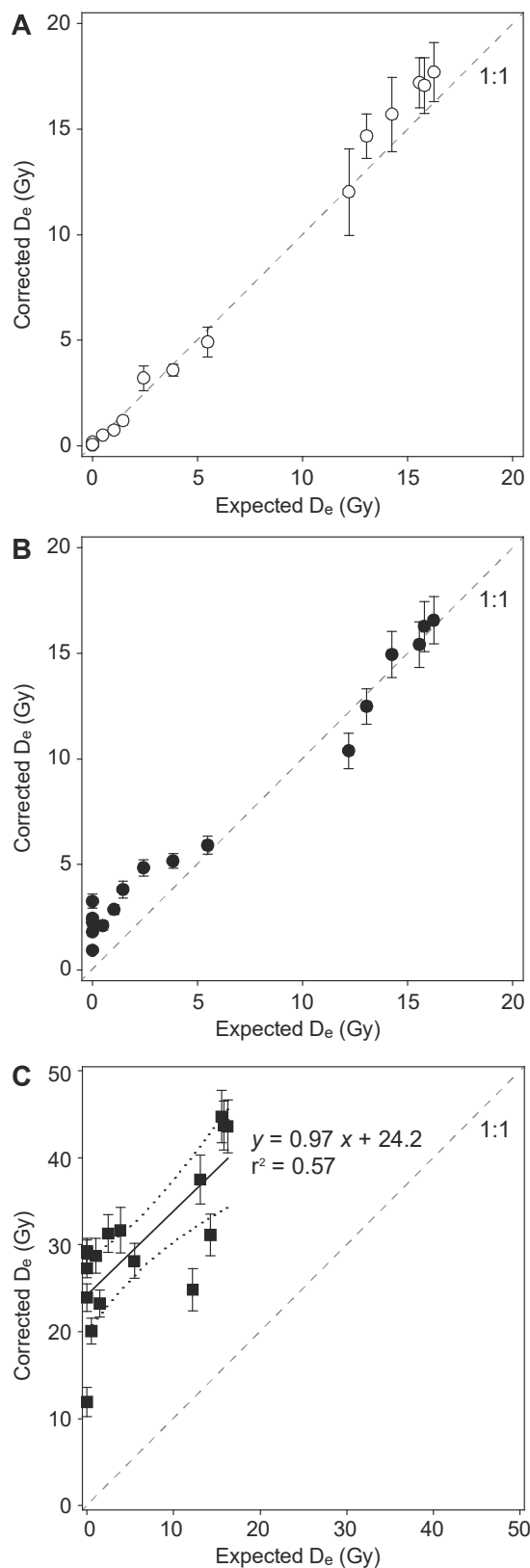

Fig. 6. *Plots of fading-corrected D$_e$ derived from (A) IR$_{50}$, (B) pIRIR$_{150}$, and (C) pIRIR$_{290}$ against expected D$_e$. The y-intercept of the regression line for pIRIR$_{290}$ represents the average residual dose, which is estimated as 24.2 Gy. Dotted lines indicate the 95% confidence interval.*

no obvious correlation with water depth. The depositional water depth of the Holocene samples is estimated from the difference between the bases of the foreshore and backshore facies, equivalent to the mean low-tide level at the time of deposition (Tamura *et al.*, 2008a), and the sample level. The relationships of the residual dose of pIRIR$_{290}$ in modern and Holocene samples with water depth exhibit no obvious trend (**Fig. 7**), but a few samples deposited in water depths shallower than 5 m show obviously lower residual doses of pIRIR$_{290}$. Along the Kujukuri coast, the upper shoreface, *i.e.*, the area shallower than 5–6 m, is characterized by frequent changes in topography caused by migration of longshore bars and troughs associated with an exchange of sand between the surf zone and the beachface (e.g., Lee *et al.*, 1998; Kuriyama, 2002; Tamura *et al.*, 2007). Samples from the foreshore and upper shoreface are likely to have been exposed to sunlight for a relatively long time, which may have bleached the difficult-to-bleach component of pIRIR$_{290}$. In the bleaching test on sample gsj15151, the residual dose of pIRIR$_{290}$ was depleted as low as 13.66±1.10 Gy after 4 h of exposure to artificial sunlight. Exposure to artificial sunlight for more than 4 h is known to further deplete pIRIR signals (e.g., Murray *et al.*, 2012). Therefore, in the beach–shoreface system at Kujukuri, sunlight bleaching of pIRIR$_{290}$ was incomplete for most of the samples; the degree of bleaching varies from sample to sample but is likely minimized in water depths <5 m.

Comparisons with other coastal systems

Examination of the bleachability of luminescence signals has generally been limited to underwater environments of coastal systems, except for river deltas. Roberts and Plater (2007) quantified the residual dose of OSL in two quartz sand samples from the modern subtidal nearshore of the Dungeness Foreland, southern England, as equivalent to 15 and 40 years. Most efforts to quantify the residual dose of coastal sediments have been made in the intertidal zone and have generally reported residual doses of quartz OSL equivalent to less than a few tens of years (e.g., Banerjee *et al.*, 2001; Ballarini *et al.*, 2003; Madsen *et al.*, 2005; Armitage *et al.*, 2006; Madsen and Murray, 2009; Brill *et al.*, 2017). Davids *et al.* (2010) reported that the K-feldspar IR$_{50}$ of modern beach sands in New England, USA, retains a residual dose corresponding to 40 years, and similar results were obtained for tidal-flat sediments on the western coast of the Korean Peninsula (Hong *et al.*, 2003). Although the quartz OSL was not investigated here, the IR$_{50}$ of Kujukuri sands is shown to have a comparable residual dose to the quartz OSL, and feldspar IRSL observed in other coastal sands.

Applications of OSL dating to deltaic systems are not limited to intertidal and supratidal sediments (e.g., Giosan *et al.*, 2006; Tamura *et al.*, 2012a, 2012b; Chamberlain *et al.*, 2018); the method can also be implemented in offshore and distributary sediments (e.g., Sugisaki *et al.*,

2015; Chamberlain *et al.*, 2017). Sugisaki *et al.* (2015) sampled suspended silts from turbid river water 300 km upstream of the Yangtze River estuary, southern China, and estimated the residual doses of quartz OSL, polymineral IR$_{50}$, and polymineral pIRIR$_{160}$ as 0.2, 1.4, and 7.4 Gy, respectively. In contrast, OSL and pIRIR$_{160}$ yielded almost identical equivalent doses for most of the samples in Holocene sediment cores collected in an offshore prodelta at 40 m water depth, which is a good indication of complete bleaching (Murray *et al.*, 2012). Thus, Sugisaki *et al.* (2015) concluded that delta sediments are well bleached by sunlight before they reach the prodelta. Chamberlain *et al.* (2017) examined the bleachability of sediments in distributaries of the Ganges–Brahmaputra–Meghna delta, Bangladesh, and reported that the OSL of fine quartz grains is generally well-bleached, whereas the pIRIR of fine polymineralic sediments is poorly bleached. They additionally observed slightly lower residual doses in grains that had been tidally reworked upstream relative to grains obtained around the river mouth and attributed this to the longer transport path and additional sunlight exposure. Gao *et al.* (2017) found nearly consistent quartz OSL and polymineralic pIRIR ages for fine sediments in a 40-m-thick Holocene subaqueous delta succession in the northern Yangtze delta plain, giving a good indication that the bleaching was sufficient. Nian *et al.* (2018) also reported consistent and precise age estimates in the Holocene Yangtze delta sediments from OSL dating of coarse-grained quartz; results from quartz appeared to be much better than radiocarbon dating, which showed many age reversals. These studies show that quartz OSL in subaqueous deltaic environments is generally well bleached and retains residual doses that are negligible in terms of millennial-scale chronology. This conclusion is also supported in other deltaic systems (Kim *et al.*, 2015; Li *et al.*, 2018b). Although quartz can be well bleached in a deltaic system, quartz grains from the Kujukuri coast are not suitable for OSL dating due to their unfavourable OSL properties.
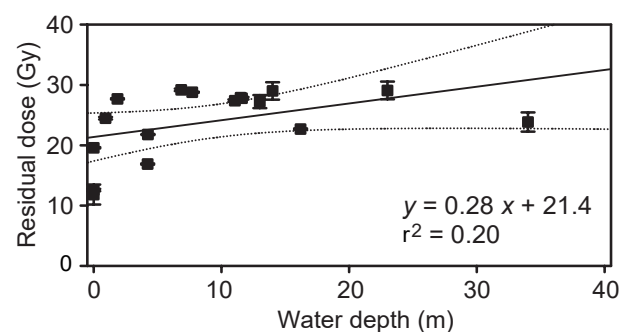

Fig. 7. *Plots of residual dose estimated for pIRIR$_{290}$ against depositional water depth of the sample. The regression line exhibits only a very weak correlation; however, a few samples taken from less than 5 m water depth exhibit slightly lower residual doses than others. Dotted lines indicate the 95% confidence interval.*

For the feldspar signal, based on comparisons with quartz OSL, Li *et al*. (2018b) estimated the residual doses of $pIRIR_{150}$ and $pIRIR_{225}$ as <5.5 Gy and 2–11 Gy, respectively, for fine polymineralic sediments from a Holocene subaqueous delta in the Bohai Sea, northeastern China. As in the Kujukuri coast, such results can be applied to clarify the possible overestimate of the pIRIR ages of Pleistocene sedimentary sequences, providing practical grounds for selecting robust feldspar signals for dating.

6. CONCLUSIONS

We quantified the residual doses of IR_{50}, $pIRIR_{150}$, and $pIRIR_{290}$ for K-feldspar sands from the modern and Holocene beach–shoreface system at Kujukuri, Pacific coast of eastern Japan. IR_{50}, defined here as the prior IRSL during $pIRIR_{150}$ measurement, of modern samples showed very low residual doses; however, $pIRIR_{150}$ retains appreciable but limited residual doses of 1–3 Gy, equivalent to 400 to 1,300 years. Generally, fading-corrected ages of IR_{50} and $pIRIR_{150}$ are reasonably consistent with radiocarbon dating in this region, whereas quartz OSL exhibits inappropriate properties for dating. Residual doses of $pIRIR_{290}$ are equivalent to >10,000 years on average, an order of magnitude greater than those of $pIRIR_{150}$, possibly leading to significant overestimation in dating Late Pleistocene sediments. Although the residual doses of $pIRIR_{290}$ show a very weak correlation with water depth, a few samples taken from the upper shoreface and foreshore are characterized by much lower residuals than the average, probably as a result of longer sunlight exposure compared to deeper environments. Empirical assessments of pIRIR residual dose in coastal sedimentary systems, as practised here at Kujukuri, are still limited, and such efforts help to improve the accuracy of pIRIR dating of late Quaternary coastal sedimentary sequences.

ACKNOWLEDGMENTS

REFERENCES

Adamiec G and Aitken MJ, 1998. Dose-rate conversion factors: update. *Ancient TL* 16: 37–46.

Armitage SJ, Botha GS, Duller GAT, Wintle AG, Rebêlo LP and Momade FJ, 2006. The formation and evolution of the barrier islands of Inhaca and Bazaruto, Mozambique. *Geomorphology* 82: 295–308, DOI 10.1016/j.geomorph.2006.05.011.

Auclair M, Lamothe M and Huot S, 2003. Measurement of anomalous fading for feldspar IRSL using SAR. *Radiation measurements* 37: 487–492, DOI 10.1016/S1350-4487(03)00018-0.

Balescu S and Lamothe M, 1994. Comparison of TL and IRSL age estimates of feldspar coarse grains from waterlain sediments. *Quaternary Science Reviews* 13: 437–444, DOI 10.1016/0277-3791(94)90056-6.

Ballarini M, Wallinga J, Murray AS, van Heteren S, Oost AP, Bos AJJ and van Eijk CWE, 2003. Optical dating of young coastal dunes on a decadal time scale. *Quaternary Science Reviews* 22: 1011–1017, DOI 10.1016/S0277-3791(03)00043-X.

Banerjee D, Murray AS and Foster IDL, 2001. Scilly Isles, UK: optical dating of a possible tsunami deposit from the 1755 Lisbon earthquake. *Quaternary Science Reviews* 20: 715–718, DOI 10.1016/S0277-3791(00)00042-1.

Bell WT, 1980. Alpha dose attenuation in quartz grains for thermoluminescence dating. *Ancient TL* 12: 4–8.

Brill D, May SM, Shah-Hosseini M, Rufer D, Schmidt C and Engel M, 2017. Luminescence dating of cyclone-induced washover fans at Point Lefroy (NW Australia). *Quaternary Geochronology* 41: 134–150, DOI 10.1016/j.quageo.2017.03.004.

Brill D, Reimann T, Wallinga J, May SM, Engel M, Riedesel S and Brückner H, 2018. Testing the accuracy of feldspar single grains to date late Holocene cyclone and tsunami deposits. *Quaternary Geochronology* 48: 91–103, DOI 10.1016/j.quageo.2018.09.001.

Buylaert JP, Murray AS, Thomsen KJ and Jain M, 2009. Testing the potential of an elevated temperature IRSL signal from K-feldspar. *Radiation Measurements* 44: 560–565, DOI 10.1016/j.radmeas.2009.02.007.

Buylaert JP, Thiel C, Murray AS, Vandenberghe DA, Yi S and Lu H, 2011. IRSL and post-IR IRSL residual doses recorded in modern dust samples from the Chinese Loess Plateau. *Geochronometria* 38: 432–440, DOI 10.2478/s13386-011-0047-0.

Buylaert JP, Jain M, Murray AS, Thomsen KJ, Thiel C and Sohbati R, 2012. A robust feldspar luminescence dating method for Middle and Late Pleistocene sediments. *Boreas* 41: 435–451, DOI 10.1111/j.1502-3885.2012.00248.x.

Buylaert JP, Murray AS, Gebhardt AC, Sohbati R, Ohlendorf C, Thiel C, Wastegård S, Zolitschka B and The PASADO Science Team, 2013. Luminescence dating of the PASADO core 5022-1D from Laguna Potrok Aike (Argentina) using IRSL signals from feldspar. *Quaternary Science Reviews* 71: 70–80, DOI 10.1016/j.quascirev.2013.03.018.

Chamberlain EL, Wallinga J, Reimann T, Goodbred Jr SL, Steckler MS, Shen Z and Sincavage R, 2017. Luminescence dating of delta sediments: Novel approaches explored for the Ganges-Brahmaputra-Meghna Delta. *Quaternary Geochronology* 41: 97–111, DOI 10.1016/j.quageo.2017.06.006.

Chamberlain EL, Törnqvist TE, Shen Z, Mauz B and Wallinga J, 2018. Anatomy of Mississippi Delta growth and its implications for coastal restoration. *Science Advances* 4: eaar4740, DOI 10.1126/sciadv.aar4740.

Cunningham AC, Tamura T and Armitage AS, 2019. Applications to coastal and marine environments. In: Handbook of Luminescence Dating (Ed. Bateman MD), Whittles Publishing, 259–292.

Davids F, Duller GA, Roberts HM, 2010. Testing the use of feldspars for optical dating of hurricane overwash deposits. *Quaternary Geochronology* 5: 125–130, DOI 10.1016/j.quageo.2009.03.001.

Durcan JA, King GE and Duller GAT, 2015. DRAC: Dose Rate and Age Calculator for trapped charge dating. *Quaternary Geochronology* 28: 54–61, DOI 10.1016/j.quageo.2015.03.012.

Fu X and Li SH, 2013. A modified multi-elevated-temperature post-IR IRSL protocol for dating Holocene sediments using K-feldspar. *Quaternary Geochronology* 17: 44–54, DOI 10.1016/j.quageo.2013.02.004.

Fuchs MC, Kreutzer S, Burow C, Dietze M, Fischer M, Schmidt C and Fuchs M, 2015. Data processing in luminescence dating analysis: an exemplary workflow using the R package 'Luminescence'.

Quaternary International 362: 8–13, DOI 10.1016/j.quaint.2014.06.034.

Galbraith RF, Roberts RG, Laslett GM, Yoshida H and Olley JM, 1999. Optical dating of single and multiple grains of quartz from jinmium rock shelter, northern australia: part 1, experimental design and statistical models. *Archaeometry* 41: 339–364, DOI 10.1111/j.1475-4754.1999.tb00987.x.

Gao L, Long H, Shen J, Yu G, Liao M and Yin Y, 2017. Optical dating of Holocene tidal deposits from the southwestern coast of the South Yellow Sea using different grain-size quartz fractions. *Journal of Asian Earth Sciences* 135: 155–165, DOI 10.1016/j.jseaes.2016.12.036.

Giosan L, Donnelly JP, Constantinescu S, Filip F, Ovejanu I, Vespremeanu-Stroe A, Vespremeanu E and Duller GAT, 2006. Young Danube delta documents stable Black Sea level since the middle Holocene: Morphodynamic, paleogeographic, and archaeological implications. *Geology* 34: 757–760, DOI 10.1130/G22587.1.

Hong DG, Choi MS, Han JH and Cheong CS, 2003. Determination of sedimentation rate of a recently deposited tidal flat, western coast of Korea, using IRSL dating. *Quaternary Science Reviews* 22: 1185–1189, DOI 10.1016/S0277-3791(03)00012-X.

Huntley DJ and Baril MR, 1997. The K content of the K-feldspars being measured in optical dating or in thermoluminescence dating. *Ancient TL* 15: 11–13.

Huntley DJ and Lamothe M, 2001. Ubiquity of anomalous fading in K-feldspars and the measurement and correction for it in optical dating. *Canadian Journal of Earth Sciences* 38: 1093–1106, DOI 10.1139/e01-013.

Kim JC, Cheong D, Shin S, Park YH and Hong SS, 2015. OSL chronology and accumulation rate of the Nakdong deltaic sediments, southeastern Korean Peninsula. *Quaternary Geochronology* 30: 245–250, DOI 10.1016/j.quageo.2015.01.006.

Komatsubara J, 2019. Sedimentary environments and basal topography of postglacial deposits in the Kujukuri coastal Plain, Boso Peninsula, central Japan. Seamless Geoinformation of Coastal Zone "Eastern Coastal Zone of Boso Peninsula", Explanatory Note, Geological Survey of Japan, National Institute of Advanced Industrial Science and Technology, 12 p.

Kreutzer S, Schmidt C, Fuchs MC, Dietze M, Fischer M and Fuchs M, 2012. Introducing an R package for luminescence dating analysis. *Ancient TL* 30: 1–8.

Kreutzer S, Schmidt C, DeWitt R and Fuchs M, 2014. The a-value of polymineral fine grain samples measured with the post-IR IRSL protocol. *Radiation Measurements* 69: 18–29, DOI 10.1016/j.radmeas.2014.04.027.

Kuriyama Y, 2002. Medium-term bar behavior and associated sediment transport at Hasaki, Japan. *Journal of Geophysical Research* 107: 3132, DOI 10.1029/2001JC000829.

Lee G, Nicholls RJ and Birkemeir WA, 1998. Storm driven variability of the beach–nearshore profile at Duck, North Carolina, USA, 1981–1991. *Marine Geology* 148: 163–177, DOI 10.1016/S0025-3227(98)00010-3.

Li B, Roberts RG and Jacobs Z, 2013. On the dose dependency of the bleachable and non-bleachable components of IRSL from K-feldspar: Improved procedures for luminescence dating of Quaternary sediments. *Quaternary Geochronology* 17: 1–13, DOI 10.1016/j.quageo.2013.03.006.

Li B, Jacobs Z, Roberts RG and Li SH, 2014. Review and assessment of the potential of post-IR IRSL dating methods to circumvent the problem of anomalous fading in feldspar luminescence. *Geochronometria* 41: 178–201, DOI 10.2478/s13386-013-0160-3.

Li F, Pan B, Lai Z, Gao H and Ou X, 2018a. Identifying the degree of luminescence signal bleaching in fluvial sediments from the Inner Mongolian reaches of the Yellow River. *Geochronometria* 45: 82–96, DOI 10.1515/geochr-2015-0087.

Li Y, Shang Z and Tsukamoto S, Tamura T, Yi L, Wang H, Frechen M, Li J and Jiang X, 2018b. Quartz and K-feldspar luminescence dating of sedimentation in the North Bohai coastal area (NE China) since the late pleistocene. *Journal of Asian Earth Sciences* 152: 103–115, DOI 10.1016/j.jseaes.2017.10.036.

Madsen AT, Murray AS, Andersen TJ, Pejrup M and Breuning-Madsen H, 2005. Optically stimulated luminescence dating of young estuarine sediments: A comparison with ^{210}Pb and ^{137}Cs dating. *Marine Geology* 214: 251–268, DOI 10.1016/j.margeo.2004.10.034.

Madsen AT, Buylaert JP and Murray AS, 2011. Luminescence dating of young coastal deposits from New Zealand using feldspar. *Geochronometria* 38: 378–390, DOI 10.2478/s13386-011-0042-5.

Madsen AT and Murray AS, 2009. Optically stimulated luminescence dating of young sediments: A review. *Geomorphology* 109: 3–16, DOI 10.1016/j.geomorph.2008.08.020.

Masuda F, Fujiwara O, Sakai T, Araya T, Tamura T and Kamataki T, 2001a. Progradation of the Holocene beach-shoreface system in the Kujukuri strand plain, Pacific coast of the Boso Peninsula, central Japan. *Daiyonki Kenkyu (Quaternary Research)* 40: 223–233.

Masuda F, Fujiwara O, Sakai T and Araya T, 2001b. Relative sea-level changes and co-seismic uplifts over six millennia, preserved in beach deposits of the Kujukuri strand plain, Pacific coast of the Boso Peninsula, Japan. *Chigaku Zasshi (Journal of Geography)* 110: 650–664.

Mejdahl V, 1979. Thermoluminescence dating: beta-dose attenuation in quartz grains. *Archaeometry* 21: 61–72, DOI 10.1111/j.1475-4754.1979.tb00241.x.

Moriwaki H, 1979. The landform evolution of the Kujukuri coastal plain, central Japan. *Daiyonki Kenkyu (Quaternary Research)* 18, 1–16.

Murray AS, Thomsen KJ, Masuda N, Buylaert JP, JainM, 2012. Identifying well-bleached quartz using the different bleaching rates of quartz and feldspar luminescence signals. *Radiation Measurements* 47: 688–695, DOI 10.1016/j.radmeas.2012.05.006.

Murray-Wallace CV, 2002. Pleistocene coastal stratigraphy, sea-level highstands and neotectonism of the southern Australian passive continental margin – a review. *Journal of Quaternary Science* 17: 469–489, DOI 10.1002/jqs.717.

Nagai T, 2002. Long term statistics report on nation wide ocean wave information network for ports and harbours (NOWPHAS 1970–1999). Technical Note of Port and Harbor Research Institute 1035: 388.

Nakada M, Yonekura N and Lambeck K, 1991. Late Pleistocene and Holocene sea-level changes in Japan: implications for tectonic histories and mantle rheology. *Palaeogeography, Palaeoclimatology, Palaeoecology* 85: 107–122, DOI 10.1016/0031-0182(91)90028-P.

Nian X, Zhang W, Wang Z, Sun Q, Chen J and Chen Z, 2018. Optical dating of Holocene sediments from the Yangtze River (Changjiang) delta, China. *Quaternary International* 467: 251–263, DOI 10.1016/j.quaint.2018.01.011.

Nishida N, Ajioka T, Ikehara K, Nakashima R and Utsunomiya M, 2019. Spatial variation and stratigraphy of the marine sediments off the east of the Boso Peninsula, Pacific Ocean, Japan. Seamless Geoinformation of Coastal Zone "Eastern Coastal Zone of Boso Peninsula", Explanatory Note, Geological Survey of Japan, National Institute of Advanced Industrial Science and Technology, 17 p.

Prescott JR and Hutton JT, 1994. Cosmic ray contributions to dose rates for luminescence and ESR dating: large depths and long-term time variations. *Radiation measurements* 23: 497–500, DOI 10.1016/1350-4487(94)90086-8.

Preusser F, Muru M and Rosentau A, 2014. Comparing different post-IR IRSL approaches for the dating of Holocene coastal foredunes from Ruhnu Island, Estonia. *Geochronometria* 41: 342–351, DOI 10.2478/s13386-013-0169-7.

Reimann T and Tsukamoto S, 2012. Dating the recent past (< 500 years) by post-IR IRSL feldspar–Examples from the North Sea and Baltic Sea coast. *Quaternary Geochronology* 10: 180–187, DOI 10.1016/j.quageo.2012.04.011.

Reimer PJ, Bard E, Bayliss A, Beck JW, Blackwell PG, Bronk Ramsey C, Buck CE, Cheng H, Edwards RL, Friedrich M, Grootes PM, Guilderson TP, Haflidason H, Hajdas I, Hatté C, Heaton TJ, Hoffmann DL, Hogg AG, Hughen KA, Kaiser KF, Kromer B, Manning SW, Niu M, Reimer RW, Richards DA, Scott EM, Southon JR, Staff RA, Turney CSM and van der Plicht J., 2013. IntCal13 and Marine13 radiocarbon age calibration curves 0–

50,000 years cal BP. *Radiocarbon* 55:1869–1887, DOI 10.2458/azu_js_rc.55.16947.

Riedesel S, Brill D, Roberts HM, Duller GA, Garrett E, Zander AM, King GE, Tamura T, Burow C, Cunningham A, Seeliger M, De Baptist M, Heyvaert VMA, Fujiwara O, Brückner H and the QuakeRecNankai Team, 2018. Single-grain feldspar luminescence chronology of historical extreme wave event deposits recorded in a coastal lowland, Pacific coast of central Japan. *Quaternary geochronology* 45: 37–49, DOI 10.1016/j.quageo.2018.01.006.

Rink WJ and Pieper KD, 2001. Quartz thermoluminescence in a storm deposit and a welded beach ridge. *Quaternary Science Reviews* 20: 815–820, DOI 10.1016/S0277-3791(00)00082-2.

Roberts HM and Plater AJ, 2007. Reconstruction of Holocene foreland progradation using optically stimulated luminescence (OSL) dating: an example from Dungeness, UK. *The Holocene* 17: 495–505, DOI 10.1177/0959683607077034.

Sohbati R, Murray AS, Buylaert JP, Ortuño M, Cunha PP and Masaa E, 2011. Luminescence dating of Pleistocene alluvial sediments affected by the Alhama de Murcia fault (eastern Betics, Spain) – a comparison between OSL, IRSL and post-IR IRSL ages. *Boreas* 41: 250–262, DOI 10.1111/j.1502-3885.2011.00230.x.

Stuiver M and Reimer PJ, 1993. Extended ^{14}C database and revised CALIB radiocarbon calibration program. *Radiocarbon* 35: 215–230.

Sugisaki S, Buylaert JP, Murray A, Tada R, Zheng H, Ke W, Saito K, Chao L, Li S and Irino T, 2015. OSL dating of fine-grained quartz from Holocene Yangtze delta sediments. *Quaternary Geochronology* 30: 226–232, DOI 10.1016/j.quageo.2015.02.021.

Tamura T, Masuda F, Sakai T and Fujiwara O, 2003. Temporal development of prograding beach–shoreface deposits: the Holocene of Kujukuri coastal plain, eastern Japan. *Marine Geology* 198: 191–207, DOI 10.1016/S0025-3227(03)00123-3.

Tamura T, Nanayama F, Saito Y, Murakami F, Nakashima R and Watanabe K, 2007. Intra-shoreface erosion in response to rapid sea-level fall: depositional record of a tectonically uplifted strand plain, Pacific coast of Japan. *Sedimentology* 54: 1149–1162, DOI 10.1111/j.1365-3091.2007.00876.x.

Tamura T, Saito Y and Masuda F, 2008a. Variations in depositional architecture of Holocene to modern prograding shorefaces along the Pacific coast of eastern Japan.In Recent Advances in Models of Siliciclastic Shallow-Marine Stratigraphy, Hampson GJ, Steel RJ, Burgess P, Dalrymple RW (eds). *SEPM Special Publication* 90: 189–203.

Tamura T, Murakami F, Nanayama F, Watanabe K and Saito Y, 2008b. Ground-penetrating radar profiles of Holocene raised-beach deposits in the Kujukuri strand plain, Pacific coast of eastern Japan. *Marine Geology* 248: 11–27, DOI 10.1016/j.margeo.2007.10.002.

Tamura T, Murakami F and Watanabe K, 2010. Holocene beach deposits for assessing coastal uplift of the northeastern Boso Peninsula, Pacific coast of Japan. *Quaternary Research* 74: 227–234, DOI 10.1016/j.yqres.2010.07.009.

Tamura T, Saito Y, Bateman MD, Nguyen VL, Ta TKO and Matsumoto D, 2012a. Luminescence dating of beach ridges for characterizing multi-decadal to centennial deltaic shoreline changes during Late Holocene, Mekong River delta. *Marine Geology* 326: 140–153, DOI 10.1016/j.margeo.2012.08.004.

Tamura T, Saito Y, Nguyen VL, Ta TKO, Bateman MD, Matsumoto D and Yamashita S, 2012b. Origin and evolution of interdistributary delta plains; insights from Mekong River delta. *Geology* 40: 303–306, DOI 10.1130/G32717.1.

Tamura T, Sawai Y and Ito K, 2015. OSL dating of the AD 869 Jogan tsunami deposit, northeastern Japan. *Quaternary Geochronology* 30: 294–298, DOI 10.1016/j.quageo.2015.06.001.

Tamura T, Ito K, Inoue T and Sakai T, 2017. Luminescence dating of Holocene beach-ridge sands on the Yumigahama Peninsula, western Japan. *Geochronometria* 44: 331–340, DOI 10.1515/geochr-2015-0076.

Thomsen KJ, Murray AS, Jain M and Bøtter-Jensen L, 2008. Laboratory fading rates of various luminescence signals from feldspar-rich sediment extracts. *Radiation Measurements* 43: 1474–1486, DOI 10.1016/j.radmeas.2008.06.002.

Tokuyasu K, Tanaka K, Tsukamoto S and Murray A, 2010. The characteristics of OSL signal from quartz grains extracted from modern sediments in Japan. *Geochronometria* 37: 13–19, DOI 10.2478/v10003-010-0020-6.

Tsukamoto S, Rink WJ and Watanuki T, 2003. OSL of tephric loess and volcanic quartz in Japan and an alternative procedure for estimating De from a fast OSL component. *Radiation Measurements* 37: 459–465, DOI 10.1016/S1350-4487(03)00054-4.

Uda T, 1989. Comparative study on long-term shoreline evolution during the past 6000 years and recent short-term beach changes on the Kujukuri coast. *Chikei (Transaction Japanese Geomorphological Union)* 10: 343–355.

Unozawa A, Oka S, Sakamoto T and Komasawa M, 1983. 1:200,000 Geological Map of Chiba. Geological Survey of Japan, 1 sheet.